Rapid Communications | Editors' Suggestion

Distinguishing Majorana bound states from localized Andreev bound states by interferometry

Michael Hell,[1,2] Karsten Flensberg,[1] and Martin Leijnse[1,2]
[1]*Center for Quantum Devices and Station Q Copenhagen, Niels Bohr Institute, University of Copenhagen, DK-2100 Copenhagen, Denmark*
[2]*Division of Solid State Physics and NanoLund, Lund University, Box 118, S-22100, Lund, Sweden*

(Received 17 October 2017; published 10 April 2018)

Experimental evidence for Majorana bound states (MBSs) is so far mainly based on the robustness of a zero-bias conductance peak. However, similar features can also arise due to Andreev bound states (ABSs) localized at the end of an island. We show that these two scenarios can be distinguished by an interferometry experiment based on embedding a Coulomb-blockaded island into an Aharonov-Bohm ring. For two ABSs, when the ground state is nearly degenerate, cotunneling can change the state of the island, and interference is suppressed. By contrast, for two MBSs the ground state is nondegenerate, and cotunneling has to preserve the island state, which leads to h/e-periodic conductance oscillations with magnetic flux. Such interference setups can be realized with semiconducting nanowires or two-dimensional electron gases with proximity-induced superconductivity and may also be a useful spectroscopic tool for parity-flip mechanisms.

DOI: 10.1103/PhysRevB.97.161401

Andreev bound states (ABSs) are coupled particle-hole excitations of superconductors bound to impurities [1–3], to their surfaces [4], or in junctions [5] with an energy in the superconducting gap. Since an ABS is a fermionic excitation, its field operator $f = \gamma_1 + i\gamma_2$ can be decomposed into a pair of Majorana operators $\gamma_1 = \gamma_1^\dagger$, $\gamma_2 = \gamma_2^\dagger$. Although the corresponding wave functions overlap in space in most cases, they can also be spatially separated for topological superconductors with triplet pairing [6–10]. This pins the energy of these Majorana bound states (MBSs) robustly to the middle of the superconducting gap and renders their non-Abelian exchange statistics accessible through braiding [11–21]. Both properties may be useful for quantum computation [22–24].

Topological superconductors may be realized in semiconductors with strong spin-orbit coupling, proximity-induced superconductivity, and magnetic fields [25,26]. Evidence for MBSs in these systems is based on a robust zero-bias conductance peak [27–36] as predicted by theory [37–41]. However, such a peak can also be caused by disorder [42], multiband effects [43], weak antilocalization [44], the Kondo effect [45], and, in particular, ABSs [46,47]. To rule out disorder effects, intensive efforts have been made to fabricate cleaner devices [48–52].

Distinguishing MBSs from ABSs is one of the most urgent goals in Majorana research. What we refer to here as ABSs are modes with a large Majorana overlap. If ABSs are extended along the island, they may be discriminated from MBSs by probing a finite conductance in the middle of the island or by a strong response to a gate affecting the middle region. However, one cannot discriminate ABSs from MBSs in this way if there are two terminal ABSs, i.e., one ABS localized at each end of an island [Fig. 1(c)]. Although the general expectation is that ABSs do not show a similar robustness against parameter variations as MBSs, ABSs can stick close to zero energy under special conditions when the longitudinal confinement potential is smooth [47,53]. This situation has to be contrasted with the desired situation of two MBSs [Fig. 1(d)] when the potential is rather uniform and rises sharply at the end of the island.

In this Rapid Communication, we show how to distinguish the case of two terminal ABSs close to zero energy from the case of two terminal MBSs by embedding a Coulomb-blockaded island into an interferometric setup [Fig. 1(a)].

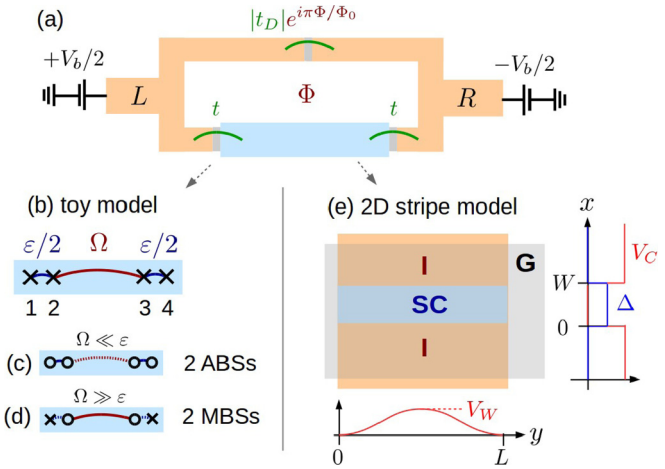

FIG. 1. Sketch of the interferometer model. (a) Two normal conducting leads (orange, labeled L and R) are connected via a superconducting island (blue) and a reference arm. (b) The toy model for the island consists of four Majoranas, tunable from (c) two terminal ABSs to (d) two terminal MBSs. (e) The two-dimensional model for a Majorana stripe as seen from the top: A stripe of a superconductor [(SC), blue] is placed on top of a semiconductor (orange) and induces a superconducting gap (blue in the side graph). A gate on top [(G), gray] induces a transverse confinement potential V_C (red in the side graph). Increasing a potential barrier V_W (red in the bottom graph) along the stripe tunes the stripe from case (d) to (c). Majoranas that are weakly (strongly) coupled to others are depicted by crosses (circles with a connecting line).

Interferometers have been proposed earlier to detect MBSs in grounded [54–59] and floating [60–64] devices and to distinguish MBSs from ABSs [59,62]. The advantages of our proposal are: (i) it relies on a standard charge current measurement, (ii) it successfully distinguishes between MBSs and ABSs also when the MBSs are not fully localized, and (iii) it can straightforwardly be implemented using current fabrication capabilities.

We focus on the case when the charging energy E_C is the dominant energy scale (besides the superconducting gap Δ) as in Majorana box qubits [65,66]. This allows us to study the transport in the cotunneling regime when the total charge on the island is fixed. This also fixes the total fermion parity of the ground state, which can be (almost) twofold degenerate in the case of two ABSs, whence it is nondegenerate for two MBSs. Thus, cotunneling processes cannot change the state of the island for two MBSs and allow for a large interference contrast. This is different from the limiting case of two localized ABSs in which the parity of both ABSs can be flipped [62]. This conserves the total fermion parity and reduces the interference contrast strongly. We show that this mechanism, captured by a toy model [Fig. 1(b)], also holds when using a microscopic two-dimensional (2D) model of the island [Fig. 1(e)] tuning between the two limits.

Toy model. Let us consider an island that hosts four Majoranas $1,\ldots,4$, two localized at each end [Fig. 1(b)]. The Hamiltonian reads

$$H_I = i\varepsilon(\gamma_1\gamma_2+\gamma_3\gamma_4) - i\Omega\gamma_2\gamma_3 + E_{C,n}, \tag{1}$$

where we included the charging energy of the island $E_{C,n} = E_C(n-n_g)^2$. Here, n is the number operator for the electrons on the island, and n_g describes the gating. The above toy model interpolates between the situation of two terminal ABSs and two terminal MBSs: When $\Omega \ll \varepsilon$, two ABSs are at energy $\approx\varepsilon$ [Fig. 1(c)]. As they are formed predominantly by the Majorana operators (γ_1,γ_2) and (γ_3,γ_4), we will denote them by $\langle 12\rangle$ and $\langle 34\rangle$, respectively. By contrast, when $\Omega \gg \varepsilon$, there are two terminal MBSs [Fig. 1(d)]. The corresponding Majorana operators (γ_1,γ_4) form a mode $\langle 14\rangle$ with a small energy $\approx\varepsilon^2/2\Omega$. In addition, the pair of Majorana operators (γ_2,γ_3) forms a mode $\langle 23\rangle$ at higher energy $\approx 2\Omega$.

Interferometer model. The interferometer is enclosed between two nonsuperconducting leads described by $H_0 = \sum_{rk\sigma}(\varepsilon_{rk}-\mu_r)c^\dagger_{rk\sigma}c_{rk\sigma}$, where $c_{rk\sigma}$ denotes the annihilator for electrons in lead $r=L,R$ in mode k with spin $\sigma = \uparrow,\downarrow$. The leads are held at a common temperature T and are voltage-biased symmetrically: $\mu_L = -\mu_R = V_b/2$ (we set $e=\hbar=c=k_B=1$).

The tunnel Hamiltonian reads

$$H_T = \sum_{rk\sigma m=1,2} c_{rk\sigma}e^{i\varphi/2}t_{r\sigma m}(\delta_{rL}\gamma_m + \delta_{rR}\gamma_{5-m}) + \sum_{kk'\sigma\sigma'} t_{D,\sigma\sigma'}c^\dagger_{Lk\sigma}c_{Rk'\sigma'} + \text{H.c.}, \tag{2}$$

where φ denotes the superconducting phase on the island and $m=1,2$ enumerates the Majorana operators. In our toy model, we assume that lead r couples only to the two nearest MBSs [the first line of Eq. (2)] with energy-independent tunnel matrix elements $t_{r\sigma m}$. For simplicity, we assume the island to be left-right symmetric so that they obey the relation $t_{L\sigma m} = (-1)^m\sigma t_{R\bar\sigma\bar m} = t_{\sigma m}$ (see the Supplemental Material [67]). By rotating the spin basis in the leads, one can parametrize the tunnel matrix elements conveniently as $t_{\uparrow 1} = t\,\cos(\lambda)$, $t_{\downarrow 1}=0$, $t_{\uparrow 2} = t\,\sin(\lambda)\cos(\beta)e^{i\delta}$, and $t_{\downarrow 2} = t\,\sin(\lambda)\sin(\beta)e^{i\delta}$ (see the Supplemental Material [67]). The parameter t together with the spin- and energy-independent density of states ν of the leads sets the overall tunnel rate $\Gamma = 2\pi\nu|t|^2$ between the leads and the island, λ characterizes the relative coupling strength of the two Majoranas to the leads, δ is a relative phase shift, and β is the canting of the different spin directions the two Majoranas couple to.

In our model, a featureless reference arm connects the two leads [the second term in Eq. (2)]. The phase of the direct tunnel amplitude $t_{D,\sigma\sigma'} = |t_D|(\delta_{\sigma\sigma'} + \tau_{\rm sf}\delta_{\sigma\bar\sigma'})e^{i\pi\Phi/\Phi_0}$ is controlled by the magnetic flux Φ threaded through the loop ($\Phi_0 = e/2h$). We neglect here decoherence in the reference arm, which is motivated by the experimental observation of phase-coherent transport up to several micrometers in InAs [51,68] and InGaAs [69] interferometers. Note that, if $\lambda = 0$ or $\beta = 0$, the island couples only to electrons with spin $\uparrow(\downarrow)$ in the left (right) lead. In the special case when the tunneling in the reference arm is spin conserving ($\tau_{\rm sf}=0$), no interference can appear because one can tell from the spin of the outgoing electron which path has been taken [70]. In practice, the island is of course not perfectly symmetric, and spin-orbit coupling rotates the spin of electrons traveling through the reference arm, resulting in a nonzero interference. For simplicity, we set $\tau_{\rm sf}=1$, which limits the interference contrast to $1/2$ when $\beta = 0$ [Eq. (4)].

Transport calculations. Our goal is to understand the behavior of the maximal interference contrast (MIC),

$$\text{MIC} := \max_{\Phi,|t_D|}\left|\frac{I(\Phi)-I(\Phi+\Phi_0)}{I(\Phi)+I(\Phi+\Phi_0)}\right|. \tag{3}$$

Here, $I(\Phi)$ is the stationary current through the interferometer. Note that the maximal or minimal current may not necessarily flow for $\Phi = 0,\pi$. Since interference requires coherent transport through the island, we constrain our calculations to the cotunneling regime. We set up a master equation (see the Supplemental Material [67]) and consider the specific situation when only one particular charge state $n=n_0$ of the island is occupied and cotunneling predominantly involves only the adjacent charge state n_0+1 ($\Gamma,T,V_b \ll U = E_{C,n_0+1} - E_{C,n_0} \ll E_{C,n_0} - E_{C,n_0-1}$). Without loss of generality, we assume n_0 to be even. While our toy model neglects cotunneling through the quasiparticle continuum, quasiparticle states are included partially later on in the 2D island model.

The cotunneling rates are computed with the T-matrix approach including terms of $O(t^2,t_D)$ into the T matrix (see the Supplemental Material [67]). We neglect all other contributions, including those leading to tunneling-induced renormalization effects or the Kondo effect ($\Gamma, T_K \ll T$) and Cooper-pair cotunneling forming a virtual intermediate Cooper pair ($\Gamma \ll U,\Delta$).

Interference contrast for the toy model. To contrast the cases of two MBSs and two ABSs, we first study the parameter dependence of the MIC for the toy model (5). When $\beta=\delta=0$

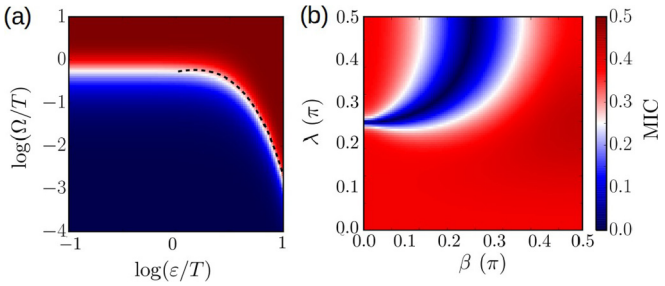

FIG. 2. Parameter dependence of the MIC for the toy model. (a) Dependence on Majorana coupling energies for $\lambda = \beta = 0$. The black-dashed line is given by $\Omega = \sqrt{2\varepsilon^3/T}e^{-\varepsilon/T}$ and marks the crossover between transport dominated by parity-conserving and parity-flipping cotunneling. (b) Dependence on tunnel matrix elements for $\Omega/T = 1$, $\varepsilon/T = 0.1$. In both cases, we used $V_b = 0.01T$, $U = 100T$, and $\delta = 0$.

and $V_b \ll E = \sqrt{\varepsilon^2 + \Omega^2} \ll U$, the MIC reads

$$\mathrm{MIC} = \frac{\tanh(E/T)}{2\sqrt{1 + \left(\frac{E/\Omega}{\cos^2(2\lambda)} - 1\right)\frac{2E/T}{\sinh(2E/T)}}}. \quad (4)$$

Details including an expression for general bias voltage are given in the Supplemental Material [67]. We see that the MIC tends to its maximal value when $\Omega/\varepsilon \gg 1$ (two MBSs), whereas it tends to zero when $\Omega/\varepsilon \ll 1$ (two ABSs) [Fig. 2(a)]. This implies that the case of two MBSs and two ABSs can be distinguished by the maximally achievable MIC. In the next two paragraphs, we explain the different behavior of the two cases when only Majoranas 1 and 4 are connected to the leads ($\lambda = 0$).

When $\Omega/\varepsilon \gg 1$ and $\Omega \gg V_b, T$, the island resides mostly in its ground state in which the parities of modes $\langle 23\rangle$ and $\langle 14\rangle$ are even. Transport is predominantly carried by parity-conserving cotunneling processes: An electron incoming from one lead flips the parity of mode $\langle 14\rangle$, and the outgoing electron flips it back. Such electrons interfere with electrons tunneling through the reference arm and lead to a large MIC [Fig. 2(a)]. The MIC is suppressed when voltage bias or temperature exceeds the inelastic cotunneling threshold, i.e., when $\min(V_b, T) > E$ [Fig. 2(a)]. In this case cotunneling processes can flip the parity of the modes $\langle 14\rangle$ and $\langle 23\rangle$ and bring the island from its ground state to the excited state. We will refer to this as parity-flipping processes (referring to the individual modes), even though the total fermion parity of the island is of course preserved. The occupation probability of the ground and excited state tends to 1/2 when $\min(V_b, T) \gg E$. Importantly, the flux dependence of the cotunneling rates differs by π depending on the initial parity of mode $\langle 23\rangle$ in the cotunneling process [60]. Hence, interference is still possible in each cotunneling event, but the MIC becomes suppressed due to averaging over both possible initial states.

When $\Omega/\varepsilon \ll 1$, the MIC can be suppressed even if $E \gg \max(V_b, T)$. The reason is that parity-conserving cotunneling is strictly forbidden in the limit $\Omega = 0$: The left lead couples only to mode $\langle 12\rangle$, whereas the right lead only couples to mode $\langle 34\rangle$. A cotunneling process transferring an electron from one to another must therefore flip the parities of both modes and thus results in the final state being different from the initial state. Hence, there is no interference. When $\varepsilon > T$, the crossover from transport dominated by parity-conserving to parity-flipping processes happens when $\Omega > \sqrt{2\varepsilon^3/T}e^{-\varepsilon/T}$ ($V_b \ll T$) [Fig. 2(a)]. In experiments, this crossover may be influenced by other processes that can flip the parities of the ABSs, such as quasiparticle poisoning from the continuum [71], Cooper-pair splitting due to photons [72], or phonons [73]. If the current is averaged over a time shorter than the time between two parity flips, interference remains detectable, and the parity of mode $\langle 23\rangle$ can be read out [65]. The MIC may thus also be utilized to measure such rates. The results we show here have to be understood as long-time averages of many parity flips instead.

The qualitative parameter dependence of the MIC remains in most cases unchanged if one considers the general case of $\lambda \neq 0$, $\beta \neq 0$, $\delta \neq 0$. From numerical calculations, we find only a weak dependence of the MIC on δ except for special points (see the Supplemental Material [67]). We find, however, a suppression of the MIC under the condition $\sqrt{(\lambda - \pi/2)^2 + \beta^2} \approx \pi/4$ [Fig. 2(b) and Eq. (4)]. Here, the parity-conserving cotunneling rates vanish because of destructive interference of processes involving only the island (not the reference arm). We finally note that the case $\Omega = 0$ with $\varepsilon = 0$ or $\lambda = 0$ is a pathological case of our model (see the Supplemental Material [67]).

Two-dimensional model for the Majorana stripe. To see whether the simple toy model discussed so far indeed captures the main physics to contrast the cases of two MBSs and two ABSs, we next turn to a more sophisticated model for the island. Following Ref. [74], we consider a Majorana stripe of width W and length L defined in a two-dimensional electron gas [Fig. 1(e)]. The electron gas is modeled by a single electron band with effective mass m^* at chemical potential μ as described by the following Bogoliubov–de Gennes Hamiltonian:

$$\mathcal{H}_{\mathrm{BdG}} = \left(-\frac{\partial_x^2 + \partial_y^2}{2m^*} + V_C(x) + V_W(y) - \mu\right)\tau_z - i\alpha(\sigma_x\partial_y - \sigma_y\partial_x)\tau_z + E_Z\sigma_y/2 + \Delta(x)\tau_x. \quad (5)$$

In the second line, we added the Rashba spin-orbit coupling (with velocity α), the Zeeman energy (E_Z) due to a magnetic field, and the induced superconducting gap. The latter is nonzero where the electron gas is covered by the superconductor: $\Delta(x) = \Delta\Theta(W/2 - |x|)$. The Hamiltonian acts on the four-component spinor $[u_\uparrow(x,y), u_\downarrow(x,y), v_\downarrow(x,y), -v_\uparrow(x,y)]^T$ containing the electron (u) and hole (v) components for spin $\sigma = \uparrow, \downarrow$. The Pauli matrices τ_i and σ_i ($i = x, y, z$) act on particle-hole and spin space, respectively. Gates are used to confine the states in the transverse direction $V_C(x) = V_C\Theta(|x| - W/2)$ ($V_C \gg \mu, \Delta, E_Z, E_{\mathrm{SO}} = m\alpha^2/2$). Equation (5) also models a nanowire if the transverse confinement in one direction is much stronger than in the other (e.g., due to gating) [75–77].

Tuning from two MBSs to two ABSs. Accounting for an additional potential profile along the stripe $V_W(y) = V_W[1 + \cos(2\pi y/L)]$, we can tune from the case of two MBSs to two ABSs by increasing V_W. Computing the energy spectrum of the island [Fig. 3(a)], we find for $V_W = 0$ only one mode ($n = 1$) close to zero energy. This mode is formed by two slightly overlapping MBSs at opposite ends of the stripe. When

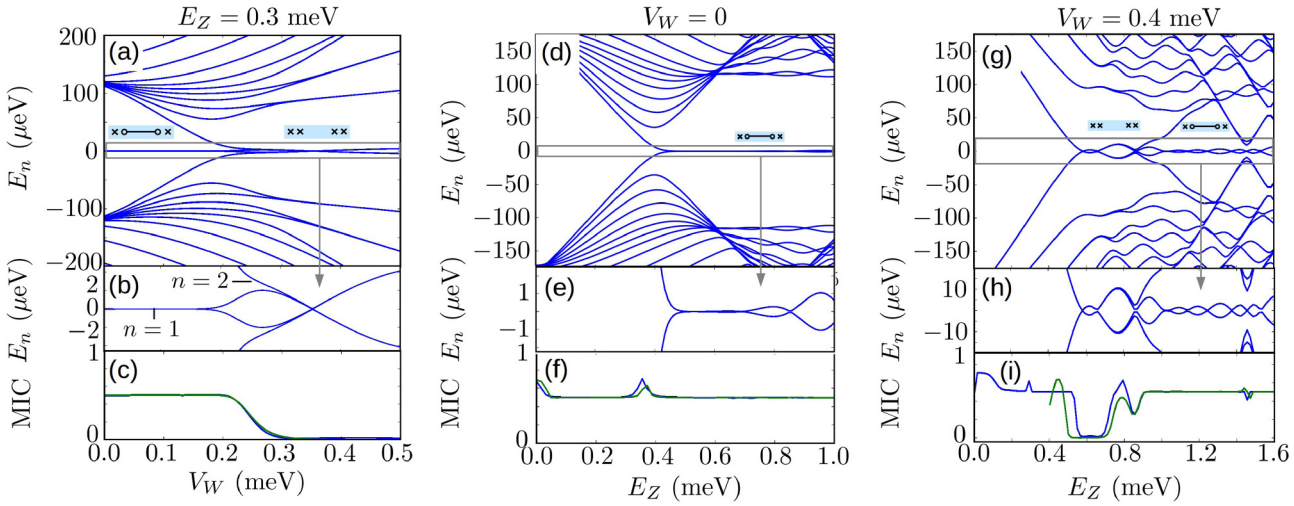

FIG. 3. Suppression of the interference contrast for the transition from two MBSs to two ABSs. We show the energy spectrum of the stripe Hamiltonian (5) (upper panels) with close-ups around zero energy (the middle panels) alongside the MIC (the lower panels). We compute the MIC both for the 2D stripe model (blue) and the toy model with parameters extracted from the 2D stripe model (green) (see the Supplemental Material [67]). The values of E_Z and V_W are specified in the panels, the lattice constant is $a = 10$ nm, $\Delta = 180$ μeV, $E_{\mathrm{SO}} = m^*\alpha^2/2 = 116.5$ μeV, $\mu = 0$, $V_C = 1$ meV, $W = 200$ nm, $L = 2$ μm, $m^* = 0.023m_e$, $U = 50$ μeV, $T = 1.6$ μeV ($\approx$20 mK), and $V_b = 1$ μeV. In (i), the toy model breaks down for $E_Z \lesssim 0.4$ meV (see the text).

increasing V_W, the second mode ($n = 2$) comes close to and sticks to zero energy [Fig. 3(b)]. When V_W is large, the two modes correspond to two ABSs localized at the ends of the wire (see the Supplemental Material [67]). The MIC is reduced when V_W is increased as the system evolves from two MBSs to two ABSs [Fig. 3(c)].

To compute the MIC using the 2D model, we include the eight lowest modes into our master equation approach. We further extracted the parameters for the toy model from the energies (yielding Ω and ε) and wave functions (yielding the tunnel matrix elements) of the two lowest modes obtained for the 2D model. In this extraction procedure (see the Supplemental Material [67]), we neglect the coupling of the Majoranas on the left (right) to the right (left) lead. We find that the toy model reproduces the MIC rather accurately.

We finally discuss the magnetic-field dependence of the MIC [Figs. 3(d)–3(i)]. Similar to the case of two MBSs, the energies of the two ABSs oscillate around zero energy as a function of the magnetic field [compare Figs. 3(e) and 3(h)]. For $V_W = 0$, we see that the MIC also stays large in the nontopological regime for small values of E_Z [Fig. 3(f)]. The reason is that parity-flipping processes are energetically forbidden as long as $2(E_1 + E_2) \ll V_b, T$. However, when E_Z is small, the Coulomb peaks are not $1e$ periodic [33], which is a way to distinguish the nontopological from the topological regime in this case.

For the case of two ABSs ($V_W = 0.4$ meV), we find that the MIC is suppressed when there are two modes close to zero energy [Fig. 3(i)]. The MIC is restored again when at least one of the modes has an energy $\gg V_b, T$. This happens for small magnetic fields [$E_Z < 0.5$ meV in Fig. 3(i)] when the ABSs are at high energies or when the case of two MBSs is restored [$E_Z > 0.9$ meV in Fig. 3(i)]. Again, for small E_Z, the Coulomb peaks are not $1e$ periodic, which rules out the presence of MBSs. We note that the toy model breaks down in this regime because Ω/ε becomes very small (leading to nearly zero current through the island). This does not happen for the full 2D model where all tunnel couplings are accounted for.

Conclusion. A zero-bias conductance peak in transport spectroscopy of superconducting islands can arise due to MBSs as well as ABSs. While extended ABSs may be probed by a contact in the middle of a superconducting stripe, terminal ABSs cannot. We have shown that terminal ABSs can instead be distinguished from two terminal MBSs by an interference experiment. Such experiments may also be useful to probe quasiparticle-poisoning rates for nonisolated islands. Finally, the idea of our approach may be of interest for initial testing of the presence of MBSs in Majorana-qubit devices [21,65] in which interferometers are integrated as a means of readout.

Acknowledgments. We acknowledge stimulating discussions with M. Deng, A. Fornieri, L. Glazman, C. M. Marcus, F. Nichele, E. O'Farrell, S. Plugge, A. Stern, A. Whiticar, and support from the Crafoord Foundation (M.L. and M.H.), the Swedish Research Council (M.L.), The Danish National Research Foundation, and from the Microsoft Station Q Program.

[1] L. Yu, Acta Phys. Sin. **21**, 75 (1965).
[2] H. Shiba, Prog. Theor. Phys. **40**, 435 (1968).
[3] A. Rusinov, Sov. Phys. JETP Lett. **9**, 85 (1969).
[4] T. Löfwander, V. Shumeiko, and G. Wendin, Supercond. Sci. Technol. **14**, R53 (2001).
[5] I. O. Kulik, Zh. Eksp.Teor. Fiz. **57**, 1745 (1970) [Sov. Phys. JETP **30**, 944 (1970)].
[6] A. Y. Kitaev, Sov. Phys. Usp. **44**, 131 (2001).
[7] J. Alicea, Rep. Prog. Phys. **75**, 076501 (2012).

[8] M. Leijnse and K. Flensberg, Semicond. Sci. Technol. **27**, 124003 (2012).
[9] C. W. J. Beenakker, Annu. Rev. Condens. Matter Phys. **4**, 113 (2013).
[10] T. D. Stanescu and S. Tewari, J. Phys.: Condens. Matter **25**, 233201 (2013).
[11] J. Alicea, Y. Oreg, G. Refael, F. von Oppen, and M. P. A. Fisher, Nat. Phys. **7**, 412 (2011).
[12] D. J. Clarke, J. D. Sau, and S. Tewari, Phys. Rev. B **84**, 035120 (2011).
[13] B. I. Halperin, Y. Oreg, A. Stern, G. Refael, J. Alicea, and F. von Oppen, Phys. Rev. B **85**, 144501 (2012).
[14] T. Hyart, B. van Heck, I. C. Fulga, M. Burrello, A. R. Akhmerov, and C. W. J. Beenakker, Phys. Rev. B **88**, 035121 (2013).
[15] D. Aasen, M. Hell, R. V. Mishmash, A. Higginbotham, J. Danon, M. Leijnse, T. S. Jespersen, J. A. Folk, C. M. Marcus, K. Flensberg *et al.*, Phys. Rev. X **6**, 031016 (2016).
[16] M. Hell, J. Danon, K. Flensberg, and M. Leijnse, Phys. Rev. B **94**, 035424 (2016).
[17] J. D. Sau, D. J. Clarke, and S. Tewari, Phys. Rev. B **84**, 094505 (2011).
[18] B. van Heck, A. R. Akhmerov, F. Hassler, M. Burrello, and C. W. J. Beenakker, New J. Phys. **14**, 035019 (2012).
[19] P. Bonderson, Phys. Rev. B **87**, 035113 (2013).
[20] S. Vijay and L. Fu, Phys. Rev. B **94**, 235446 (2016).
[21] T. Karzig, C. Knapp, R. M. Lutchyn, P. Bonderson, M. B. Hastings, C. Nayak, J. Alicea, K. Flensberg, S. Plugge, Y. Oreg *et al.*, Phys. Rev. B **95**, 235305 (2017).
[22] S. Bravyi and A. Kitaev, Ann. Phys. (N.Y.) **298**, 210 (2002).
[23] S. Bravyi and A. Kitaev, Phys. Rev. A **71**, 022316 (2005).
[24] M. H. Freedman, A. Kitaev, M. J. Larsen, and Z. Wang, Bull. New Ser. Am. Math. Soc. **40**, 31 (2003).
[25] Y. Oreg, G. Refael, and F. von Oppen, Phys. Rev. Lett. **105**, 177002 (2010).
[26] R. M. Lutchyn, J. D. Sau, and S. Das Sarma, Phys. Rev. Lett. **105**, 077001 (2010).
[27] V. Mourik, K. Zuo, S. M. Frolov, S. R. Plissard, E. P. A. M. Bakkers, and L. P. Kouwenhoven, Science **336**, 1003 (2012).
[28] A. Das, Y. Ronen, Y. Most, Y. Oreg, M. Heiblum, and H. Shtrikman, Nat. Phys. **8**, 887 (2012).
[29] A. D. K. Finck, D. J. Van Harlingen, P. K. Mohseni, K. Jung, and X. Li, Phys. Rev. Lett. **110**, 126406 (2013).
[30] L. P. Rokhinson, X. Liu, and J. K. Furdyna, Nat. Phys. **8**, 795 (2012).
[31] M. T. Deng, C. L. Yu, G. Y. Huang, M. Larsson, P. Caroff, and H. Q. Xu, Nano Lett. **12**, 6414 (2012).
[32] H. O. H. Churchill, V. Fatemi, K. Grove-Rasmussen, M. T. Deng, P. Caroff, H. Q. Xu, and C. M. Marcus, Phys. Rev. B **87**, 241401 (2013).
[33] S. M. Albrecht, A. P. Higginbotham, M. Madsen, F. Kuemmeth, T. S. Jespersen, J. Nyg, P. Krogstrup, and C. M. Marcus, Nature (London) **531**, 206 (2016).
[34] M. Deng, S. Vaitiekėnas, E. B. Hansen, J. Danon, M. Leijnse, K. Flensberg, J. Nygård, P. Krogstrup, and C. M. Marcus, Science **354**, 1557 (2016).
[35] H. J. Suominen, M. Kjaergaard, A. R. Hamilton, J. Shabani, C. J. Palmstrøm, C. M. Marcus, and F. Nichele, Phys. Rev. Lett. **119**, 176805 (2017).
[36] F. Nichele, A. C. Drachmann, A. M. Whiticar, E. C. O'Farrell, H. J. Suominen, A. Fornieri, T. Wang, G. C. Gardner, C. Thomas, A. T. Hatke *et al.*, Phys. Rev. Lett. **119**, 136803 (2017).
[37] C. J. Bolech and E. Demler, Phys. Rev. Lett. **98**, 237002 (2007).
[38] K. T. Law, P. A. Lee, and T. K. Ng, Phys. Rev. Lett. **103**, 237001 (2009).
[39] K. Flensberg, Phys. Rev. B **82**, 180516 (2010).
[40] A. Golub and B. Horovitz, Phys. Rev. B **83**, 153415 (2011).
[41] M. Wimmer, A. R. Akhmerov, J. P. Dahlhaus, and C. W. J. Beenakker, New J. Phys. **13**, 053016 (2011).
[42] D. Bagrets and A. Altland, Phys. Rev. Lett. **109**, 227005 (2012).
[43] J. Liu, A. C. Potter, K. T. Law, and P. A. Lee, Phys. Rev. Lett. **109**, 267002 (2012).
[44] D. I. Pikulin, J. P. Dahlhaus, M. Wimmer, H. Schomerus, and C. W. J. Beenakker, New J. Phys. **14**, 125011 (2012).
[45] D. Goldhaber-Gordon, H. Shtrikman, D. Mahalu, D. Abusch-Magder, U. Meirav, and M. Kastner, Nature (London) **391**, 156 (1998).
[46] E. J. H. Lee, X. Jiang, R. Aguado, G. Katsaros, C. M. Lieber, and S. De Franceschi, Phys. Rev. Lett. **109**, 186802 (2012).
[47] G. Kells, D. Meidan, and P. W. Brouwer, Phys. Rev. B **86**, 100503 (2012).
[48] P. Krogstrup, N. L. B. Ziino, W. Chang, S. M. Albrecht, M. H. Madsen, E. Johnson, J. Nygård, C. M. Marcus, and T. S. Jespersen, Nature Mater. **14**, 400 (2015).
[49] W. Chang, S. M. Albrecht, T. S. Jespersen, F. Kuemmeth, P. Krogstrup, J. Nygård, and C. M. Marcus, Nat. Nanotechnol. **10**, 232 (2015).
[50] H. Zhang, Ö. Gül, S. Conesa-Boj, M. P. Nowak, M. Wimmer, K. Zuo, V. Mourik, F. K. de Vries, J. van Veen, M. W. de Moor *et al.*, Nat. Commun. **8**, 16025 (2017).
[51] S. Gazibegovic, D. Car, H. Zhang, S. C. Balk, J. A. Logan, M. W. de Moor, M. C. Cassidy, R. Schmits, D. Xu, G. Wang *et al.*, Nature (London) **548**, 434 (2017).
[52] O. Gül, H. Zhang, F. K. de Vries, J. van Veen, K. Zuo, V. Mourik, S. Conesa-Boj, M. P. Nowak, D. J. Van Woerkom, M. Quintero-Pérez *et al.*, Nano Lett. **17**, 2690 (2017).
[53] C.-X. Liu, F. Setiawan, J. D. Sau, and S. Das Sarma, Phys. Rev. B **96**, 054520 (2017).
[54] C. Benjamin and J. K. Pachos, Phys. Rev. B **81**, 085101 (2010).
[55] S. En-Ming, P. Yi-Ming, S. Lu-Bing, and W. Bai-Gen, Chin. Phys. B **23**, 057201 (2014).
[56] B. Y. Sun and M. W. Wu, New J. Phys. **16**, 073045 (2014).
[57] A. Ueda and T. Yokoyama, Phys. Rev. B **90**, 081405 (2014).
[58] A. Ueda and T. Yokoyama, Phys. Procedia **58**, 182 (2014).
[59] K. M. Tripathi, S. Das, and S. Rao, Phys. Rev. Lett. **116**, 166401 (2016).
[60] L. Fu, Phys. Rev. Lett. **104**, 056402 (2010).
[61] A. Yamakage and M. Sato, Physica E **55**, 13 (2014).
[62] J. D. Sau, B. Swingle, and S. Tewari, Phys. Rev. B **92**, 020511 (2015).
[63] S. Rubbert and A. R. Akhmerov, Phys. Rev. B **94**, 115430 (2016).
[64] C.-K. Chiu, J. D. Sau, and S. Das Sarma, Phys. Rev. B **97**, 035310 (2018).
[65] S. Plugge, A. Rasmussen, A. Egger, and K. Flensberg, New J. Phys. **19**, 012001 (2017).
[66] S. Plugge, L. A. Landau, E. Sela, A. Altland, K. Flensberg, and R. Egger, Phys. Rev. B **94**, 174514 (2016).
[67] See Supplemental Material at http://link.aps.org/supplemental/10.1103/PhysRevB.97.161401 for more details on the models,

the density-matrix approach including some calculations, and further discussion of the results for the toy model.

[68] C. H. Yang, M. J. Yang, K. A. Cheng, and J. C. Culbertson, Phys. Rev. B **66**, 115306 (2002).

[69] S. L. Ren, J. J. Heremans, C. K. Gaspe, S. Vijeyaragunathan, T. D. Mishima, and M. B. Santos, J. Phys.: Condens. Matter **25**, 435301 (2013).

[70] H. Akera, Phys. Rev. B **47**, 6835 (1993).

[71] A. P. Higginbotham, S. M. Albrecht, G. Kirsanskas, W. Chang, F. Kuemmeth, P. Krogstrup, T. S. Jespersen, J. Nygard, K. Flensberg, and C. M. Marcus, Nat. Phys. **11**, 1017 (2015).

[72] L. Bretheau, C. O. Girit, C. Urbina, D. Esteve, and H. Pothier, Phys. Rev. X **3**, 041034 (2013).

[73] U. Patel, I. V. Pechenezhskiy, B. Plourde, M. Vavilov, and R. McDermott, Phys. Rev. B **96**, 220501 (2017).

[74] M. Hell, M. Leijnse, and K. Flensberg, Phys. Rev. Lett. **118**, 107701 (2017).

[75] R. M. Lutchyn, T. D. Stanescu, and S. Das Sarma, Phys. Rev. Lett. **106**, 127001 (2011).

[76] A. C. Potter and P. A. Lee, Phys. Rev. Lett. **105**, 227003 (2010).

[77] T. D. Stanescu, R. M. Lutchyn, and S. Das Sarma, Phys. Rev. B **84**, 144522 (2011).